

# Effective UVGI System Design Through Improved Modeling

**W.J. Kowalski, P.E.**  
Student Member ASHRAE

**William P. Bahnfleth, Ph.D., P.E.**  
Member ASHRAE

## ABSTRACT

*This paper summarizes an improved methodology for predicting the rate of airstream disinfection for UVGI systems that will enable effective designs and lower energy costs. This approach uses radiative view factors to define the three-dimensional intensity field for lamps and reflective surfaces inside enclosures. Lamp photosensor data for a variety of lamps are shown to agree more closely with the view factor model than with models using the Inverse Square Law. The intensity field due to reflectivity from internal surfaces is determined by assuming diffuse reflectivity. An analytical method is used to determine the inter-reflection component of intensity due to multiple internal reflections. The superposition of these components yields a three-dimensional intensity field matrix that can be used to calculate disinfection rates for any given microbial rate constant. Results from laboratory bioassays using *S. marcescens* in various duct configurations have corroborated model predictions within  $\pm 15\%$  in most cases.*

## INTRODUCTION

Currently available design information has not guaranteed predictable performance for UVGI air disinfection systems. Some of today's design practices can overdesign systems, leading to prohibitive costs and high energy consumption. Other design practices lead to undersized and ineffective systems. Design practices have not changed in decades, and it is worthwhile to review the history of UVGI applications to discover how this situation has come to be.

Although the first UVGI water disinfection system was implemented in 1909 (AWWA 1971), the first UVGI systems designed for airstream disinfection weren't implemented until the 1930s (Sharp 1940). Based on limited laboratory data and

using newly available UVGI lamps, these systems were sized without the benefit of preexisting criteria. Tests, either air sampling or epidemiological, were used to determine their efficacy. Some of these systems were highly successful, such as those used to control measles in schools, and one used by Riley to eliminate TB bacilli from hospital ward exhaust air (Riley and O'Grady 1961).

Other designs appeared to be ineffective, with the result that the initial glowing reviews of this technology became tempered. Guidelines were issued that sanctioned the use of UVGI only in combination with HEPA filters (Luciano 1977; ASHRAE 1991). No studies were ever undertaken to determine the root cause for any UVGI system failures. Apart from improvements in lamp designs, applications technology for airstream disinfection has remained almost stagnant for decades.

The first design guidelines for UVGI airstream disinfection systems were developed in the 1940s (Luckiesh and Holladay 1942; Luckiesh 1946). Versions appeared in catalogs that continue to be reproduced and used today (Philips 1985). These guidelines offer procedures, charts, and tables to size lamps and reflective surfaces so as to obtain a desired disinfection rate. These sizing methods, though admirably detailed for the period, suffer from a number of deficiencies:

1. They fail to define the intensity field, instead merely using the lamp rating or else relying on photometric data for lamp midpoints.
2. Lamps are specified without regard to lamp location or type.
3. The correction factor for rectangular ducts ignores the intensity field variations due to surface reflectivity.

---

**W.J. Kowalski** is a doctoral candidate and **William P. Bahnfleth** is an associate professor in the Department of Architectural Engineering, Pennsylvania State University, University Park, Pa.

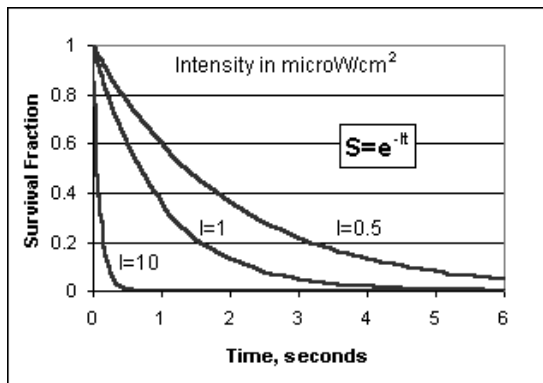
4. The relative humidity correction relies on limited studies for *E. coli* only, ignoring other studies.
5. The correction factors for reflectivity ignore duct dimensions and lengths.
6. The temperature correction chart is based on a single model of lamp and does not apply to other manufacturers' lamps.
7. These methods are based on a rate constant for *E. coli* from plate studies only.

Other manufacturers size systems by rules of thumb, such as filling the available cross section with an array of lamps, or base designs on proprietary testing. A number of sources refer to the Inverse Square Law (ISL) as defining the intensity field of UVGI lamps, but this model may be insufficiently accurate for system design and can result in systems that are underdesigned or overdesigned. Overdesigned systems, although conservative, may have prohibitive economics or, if installed, may waste energy. No current paper provides any rigorous methodology for designing and predicting the airstream disinfection rate of UVGI systems.

The net result of the various inaccuracies detailed above would, in general, result in oversized systems for most applications. However, ignoring the placement of lamps could result in systems that are both oversized (in terms of total wattage) and less effective than they could be. Energy savings could be achieved through improvement of these design methodologies, as well as lowered first costs.

It is the purpose of this paper to present a detailed method for the design of UVGI airstream disinfection systems that accounts for, or at least bounds, all the variables that may impact effectiveness. It is furthermore shown that these methods are not too complex for practical application and that the knowledge of the principles involved can contribute to a deeper understanding of what constitutes an effective UVGI system.

Finally, it is demonstrated through a series of laboratory tests that the model described here can be reasonably effective in predicting system performance. Areas where research is continuing and areas that require further research are identified.



## MODELING UVGI SYSTEMS

Four computational aspects of UVGI are essential for the accurate modeling of airstream disinfection systems—the exponential decay curve, the lamp intensity field, the direct reflected intensity field, and the inter-reflected intensity field. These will be addressed in succession, after which the topics of velocity profiles and lamp placement will be discussed.

### The Exponential Decay Curve

Ultraviolet radiation in the range 2250-3020 angstroms is lethal to microorganisms and is referred to as ultraviolet germicidal irradiation (UVGI). Microorganisms exposed to UVGI experience an exponential decrease in population similar to other methods of disinfection such as with biocides or heating (Riley and Nardell 1989; Collins 1971; Sharp 1939). The population decrease due to exposure to UVGI is described by the exponential decay equation:

$$S(t) = e^{-k_o t} \quad (1)$$

where

- $S(t)$  = population fraction at time  $t$ ,
- $k_o$  = overall decay rate constant,  $s^{-1}$ ,
- $t$  = time, s.

The exponential decay curve described by Equation 1 is known as the survival curve or the inactivation curve. The overall decay rate constant  $k_o$  defines the sensitivity of a microorganism to UVGI and is unique to each microbial species (Hollaender 1943; Jensen 1964). Figure 1a illustrates generic decay curves for a population exposed to lethal levels of UVGI irradiation.

The overall decay rate constant  $k_o$  increases linearly as a function of UVGI dose (Rentschler and Nagy 1940; Gates 1929). Therefore, the effect of intensity can be made explicit in Equation 1 by introducing a decay rate constant defined to be the rate of change of  $k_o$  with intensity:

$$S(t) = e^{-I t} \quad (2)$$

where

- $k$  = decay rate constant ( $cm^2/\mu W \cdot s$ ) and
- $I$  = intensity of UVGI irradiation ( $\mu W/cm^2$ ).

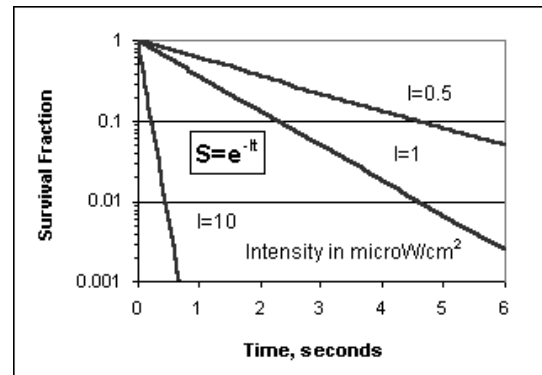


**Figure 1** Survival curve of a population exposed to UVGI at different intensities, in linear and logarithmic scales.

**TABLE 1**  
**Units of Intensity and Dose**

| Conversion Factors for Intensity<br>(Read down from units to grey block and then horizontally for conversion factor.)                         |                             |                                |                             |                           |
|---|-----------------------------|--------------------------------|-----------------------------|---------------------------|
| <b>W/m<sup>2</sup></b>  | <b>erg/mm<sup>2</sup>·s</b> | <b>microW/cm<sup>2</sup></b>   | <b>erg/cm<sup>2</sup>·s</b> | <b>W/ft<sup>2</sup></b>   |
| <b>microW/mm<sup>2</sup></b>  |                             |                                |                             |                           |
| <b>J/m<sup>2</sup>·s</b>  |                             |                                |                             |                           |
| 1   | 10                          | 100                            | 1000                        | 0.107639                  |
| 0.1   | 1                           | 10                             | 100                         | 0.010764                  |
| 0.01  | 0.1                         | 1                              | 10                          | 0.001076                  |
| 0.001   | 0.01                        | 0.1                            | 1                           | 0.000108                  |
| 9.29  | 92.90                       | 929.0                          | 9290                        | 1                         |
| <b>J/m<sup>2</sup></b>  | <b>erg/mm<sup>2</sup></b>   | <b>microW·s/cm<sup>2</sup></b> | <b>erg/cm<sup>2</sup></b>   | <b>W·s/ft<sup>2</sup></b> |
| <b>W·s/m<sup>2</sup></b>  |                             |                                |                             |                           |
| <b>microW·s/mm<sup>2</sup></b>  |                             |                                |                             |                           |
| Conversion Factors for Dose at an Exposure Time of 1 second<br>(Read up from units to grey block and then horizontally for unit equivalence.) |                             |                                |                             |                           |

An alternative interpretation of  $k$  is that it is equal in magnitude to the overall decay constant for unit intensity, which is an intensity of  $1 \mu\text{W}/\text{cm}^2$ . The preferred units for use in all of these calculations are  $\mu\text{W}/\text{cm}^2$  for intensity and  $\mu\text{W}\cdot\text{s}/\text{cm}^2$  for dose. Table 1 has been provided to dispel confusion regarding the proper units and unit conversions.

Figure 1b illustrates the effect of UVGI intensity on the decay of an exposed population of microorganisms, shown in log scale. Values of 0.5 and  $10 \mu\text{W}/\text{cm}^2$  are compared against the baseline condition of  $1 \mu\text{W}/\text{cm}^2$ . This curve is generic and represents no specific microorganism. Equation 2 represents a simplification of microbial response to UVGI but is a good approximation in most cases.

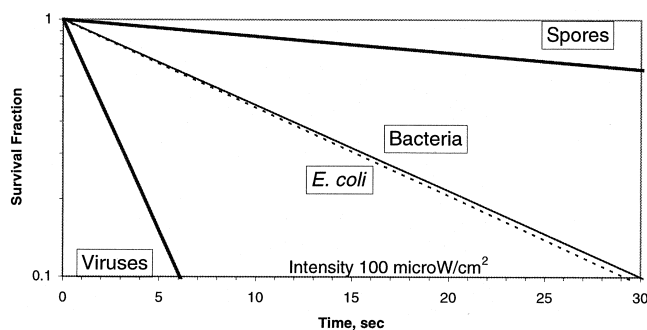
Rate constants for a wide variety of airborne pathogens are available in the literature, although these are mainly plate (petri dish cultures) or water-based rate constants. It has been noted by various investigators (Luckiesh 1946) that the rate constants in air are anywhere from four to ten times higher than those from plates or water-based studies. The use of rate constants from plate or water-based studies can result in over-design of airstream disinfection systems, although they would be appropriate for control of microbial growth on surfaces such as cooling coils.

Figure 2 illustrates the comparative susceptibility to UVGI of the three microbial groups, viruses, bacteria, and spores. This chart is based on averaged rate constants, a procedure that would be incorrect for design purposes but that provides an illustrative comparison. The spores include both fungal spores and bacterial spores. The spores are seen to be resistant to UVGI while the viruses are highly vulnerable.

Also shown in Figure 2 is the response of *E. coli*, which is not an airborne pathogen but is commonly used as

a benchmark for UVGI design. The rate constant for *E. coli* is  $0.0007675 \text{ cm}^2/\mu\text{W}\cdot\text{s}$  based on 90% kill at a dose of  $3000 \mu\text{W}\cdot\text{s}/\text{cm}^2$  (Philips 1985). This rate constant is, however, based on plate studies, not airborne studies. The rate constant for *E. coli* in air is four times higher than it is on plates (Sharp 1939, 1940).

*E. coli* may not be the best choice for airborne testing since it is not a true airborne pathogen. Airborne pathogens have evolved airborne survival mechanisms, including improved ability to resist dehydration. A better design basis microbe for airstream disinfection systems may be *Serratia marcescens*. It has rate constants that are nearly the same as those of *E. coli*, and it is a true airborne pathogen, although a relatively harmless one. Based on data from independent laboratory tests, the rate constant for *Serratia marcescens* is  $0.000718 \text{ cm}^2/\mu\text{W}\cdot\text{s}$  on plates and  $0.00291 \text{ cm}^2/\mu\text{W}\cdot\text{s}$  in air. This represents an approximate fourfold increase in rate constant from plates to air, the same as with *E. coli*.



**Figure 2** Comparison of average UVGI rate constants for viruses, bacteria, and spores.

In almost all studies that involve population decay due to UVGI or other means, a small portion of the surviving population demonstrates a much higher resistance (Cerf 1977; Whiting 1991). Typically, over 99% of the microbial population will succumb rapidly to the effects of chemicals, heat; or radiation, and a remaining fractional percentage will survive extended exposure (Davidovich and Kishchenko 1991; Qualls and Johnson 1983).

The unusually high resistance of a segment of the population may have any number of causes, for example, genetic variation or physical clumping. One current theory holds that a genetically prescribed fraction of any microbial population will remain in a state of dormancy as a hedge against evolutionary adversity (Koch 1995). Regardless of the cause, the result is always a two-stage inactivation curve with a tiny fraction of the population remaining resistant to biocidal factors.

The two-stage curve is simply the sum of a rapid decay curve (the vulnerable majority) and a slow decay curve (the resistant minority), as illustrated in Figure 3. The two-stage decay curve can be written, based on Equation 2,

$$S(t) = Fe^{-k_f t} + (1 - F)e^{-k_s t} \quad (3)$$

where

- $k_f$  = rate constant for first population,
- $k_s$  = rate constant for second population,
- $F$  = fast decaying fraction of initial population.

In addition, many microbial decay curves exhibit a decay curve shoulder (time-delayed response) when exposed to UVGI. Spores, in particular, can exhibit a pronounced shoulder when exposed to relatively low levels of intensity. For applications where microbial growth control is to be accomplished with sustained low levels of UVGI, the shoulder should be included for design purposes. Some limited data exist from which shoulder characteristics for spores can be inferred (Asthana and Tuveson 1992; Sharp 1939). Insufficient data exist to quantify either the shoulder or the second stage for most other microorganisms, and, therefore, these matters will be left for future research. The simple single-stage decay curve defined by Equation 1 will be used for the purposes of this study.

The question of the effect of relative humidity also remains unresolved. Increased relative humidity (RH) is commonly believed to decrease the decay rate under UV exposure. This may be, at best, a selective conclusion. Riley and Kaufman (1972) found that *Serratia marcescens* experiences increased resistance to UVGI at higher RH. However, Lidwell and Lowbury (1950) observed the opposite reaction for *Streptococcus pyogenes*—the resistance to UVGI increased significantly with decreasing RH. Some studies done on *E. coli* showed increased resistance with increasing RH while others failed to demonstrate any relationship with RH at all (Rentschler and Nagy 1940). A serious need exists for further study of the effects of RH on rate constants since this factor can amplify or inhibit the effects of UVGI.

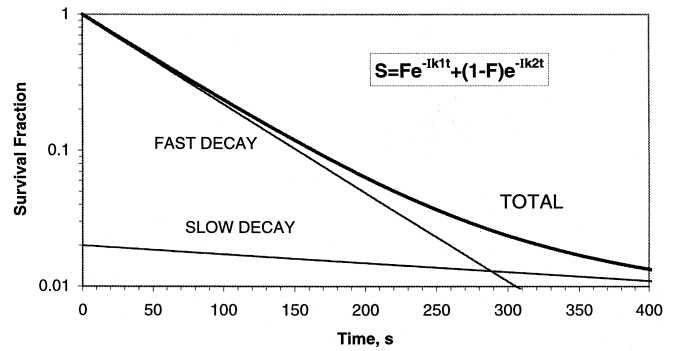


**Figure 3** Two-stage survival curve showing contribution from fast decay and slow decay populations.

### The Lamp Intensity Field

The dose received by any airborne microorganism is dependent on the lamp intensity field through which it passes. Computation of the intensity field is essential for the sizing of any system. If the entire intensity field can be established and reduced to a single value for average intensity, then the sizing will be greatly simplified.

The Inverse Square Law (IES 1981) is often used to compute the intensity of light at any distance from a lamp. This is adequate for lighting purposes but is inaccurate in the near field where much of the germicidal effect occurs. In water-based systems the ISL can be effective, but the attenuation of UVGI by water plays a larger part than the lamp geometry (Qualls and Johnson 1983, 1985; Severin et al. 1983). In air, where there is negligible attenuation of UVGI, the ISL fails to account for the lamp diameter and is at best an approximation. Even numerical integration of the ISL to create a line source fails to result in agreement with photosensor data. A more accurate approach, and one that fully accounts for lamp geometry, is to use radiation view factors.

The radiation view factor represents the fraction of diffuse radiative energy emitted by one surface that is absorbed by another surface. It defines the geometric relationship between the emitting and the receiving surface. If the emitting surface is at a constant intensity and the receiving surface is a differential element, then the view factor can be used to determine the intensity at the location of the differential element. If the receiving surface is a finite area or the emitting surface is not uniform, then the relationship can be integrated over the respective surfaces to find the total radiation absorbed.

The intensity at an arbitrary point outside a UVGI lamp can be computed using the radiation view factor from a differential planar element to a finite cylinder when the element is perpendicular to the cylinder axis and located axially at one end of the cylinder (Modest 1993):

$$F_{d1-2}(x, l, r) = \frac{L}{\pi H} \left[ \frac{1}{L} \text{ATAN}\left(\frac{L}{\sqrt{H^2-1}}\right) - \text{ATAN}\left(\sqrt{\frac{H-1}{H+1}}\right) + \frac{X-2H}{\sqrt{XY}} \text{ATAN}\left(\sqrt{\frac{X(H-1)}{Y(H+1)}}\right) \right] \quad (4)$$

The parameters in the above equation are defined as follows:

$$\begin{aligned} H &= x/r \\ L &= l/r \\ X &= (1-H)^2 + L^2 \\ Y &= (1+H)^2 + L^2 \end{aligned}$$

where

- $x$  = distance from the lamp (cm)
- $l$  = length of the lamp segment, (cm)
- $r$  = radius of the lamp, (cm)

The success of the view factor model in predicting lamp intensity fields is demonstrated in comparisons with photosensor data in Figures 4 and 5.

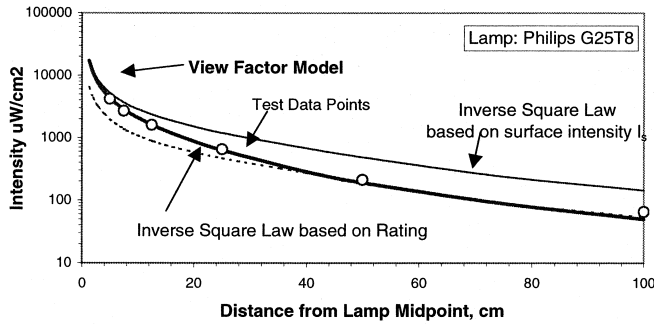


**Figure 4** Comparison of view factor model with lamp data and inverse square law.

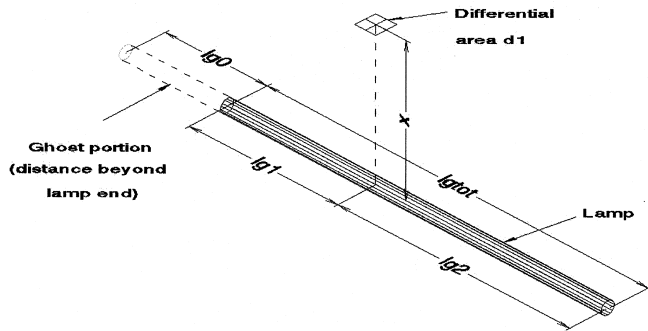


**Figure 6** View factor model of lamp showing the lamp modeled in two segments of lengths  $lg_1$  and  $lg_2$ , either of which could represent the distance along the lamp axis at which the element is located. The ghost portion represents the distance an element is located beyond the lamp ends.

To compute the view factor along the axis of the lamp at any radial distance from the axis, the lamp must be divided into two segments of lengths  $l_1$  and  $l_g - l_1$ , the sum of which will be the total lamp length  $l_g$  as shown in Figure 6. This process is known as view factor algebra. The total view factor at any point will be

$$F_{tot}(x, l_1, l_g, r) = F_{d1-2}(x, l_1, r) + F_{d1-2}(x, l_g - l_1, r). \quad (5)$$

To compute the view factor for a point beyond the ends of the lamp, an imaginary lamp must be constructed from the real portion of length  $l_g$  and a “ghost” portion of some length equivalent to the distance beyond, or before, the end of the lamp  $l_b$ . The view factor of the ghost portion is then subtracted from the total as follows:

$$F_{tot}(x, l_b - l_g, l_g, r) = F_{d1-2}(x, l_b + l_g, r) + F_{d1-2}(x, l_b, r) \quad (6)$$

An example of the above model compared with lamp data and with the ISL is shown in Figure 7. Discrepancies that exist here between the view factor model and the data may be due to errors in the photosensor readings.

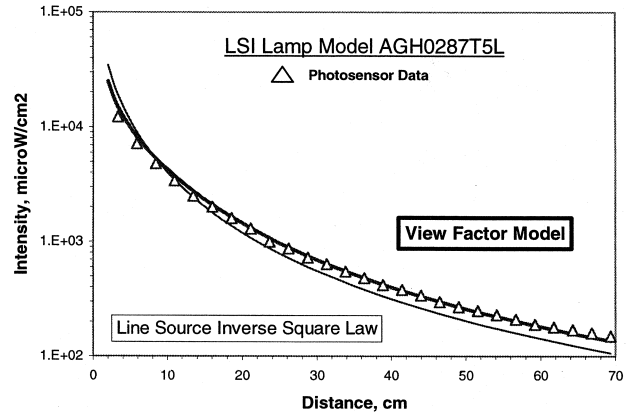


**Figure 5** Comparison of view factor model with lamp data and inverse square law.

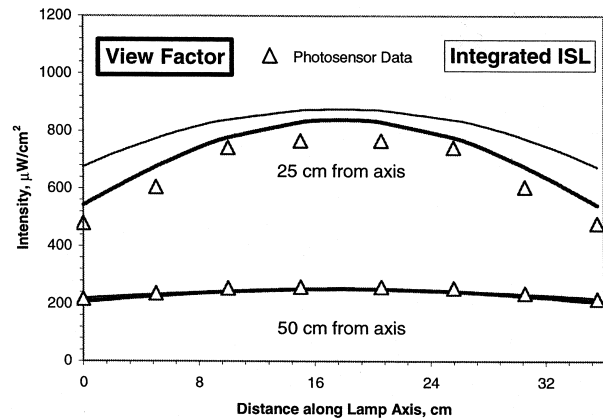


**Figure 7** Comparison of lamp data and models for intensity along the length of a lamp.

The intensity at any point will be the product of the surface intensity  $I_s$  and the total view factor. The lamp surface intensity is the UV power output divided by the lamp surface area. The intensity field at any coordinate,  $x$ ,  $y$ , or  $z$ , will be described by

$$I_s = \frac{E_{uv} F_{tot}}{2\pi r l} \quad (7)$$

where

$$I_s = \text{UV intensity at any } (x,y,z) \text{ point, } \mu\text{W}/\text{cm}^2, \text{ and}$$

$$E_{uv} = \text{UV power output of lamp, } \mu\text{W.}$$

Equations 4 through 7 can be used to create a three-dimensional matrix defining the intensity field around a lamp in any enclosure. This matrix can then be used to determine the dose received by a passing airborne microorganism, either by averaging the field intensity or by integrating the dose along airflow streamlines.

### The Reflected Intensity Field

Reflective materials, such as aluminum or magnesium oxide, can boost the intensity field both from direct reflections and from inter-reflections. The intensity field due to reflectivity depends on surface geometry and the field of the lamp. Some lamps include fixtures that are themselves reflective surfaces. Although the model developed here is considered to be a naked lamp in a rectangular enclosure, the same principles apply to the reflective surfaces of the fixtures.

Assuming the surfaces to be purely diffuse reflectors, view factors can be used to compute the intensity field for the first reflection. This assumption is not unreasonable, even for specular surfaces, provided the intensity field is relatively uniform (i.e., no hot spots in the intensity contour).

The direct intensity at each surface is determined with Equation 7. Averaging the surface intensity to simplify computations may be possible provided the intensity distribution on the wall is relatively even. Otherwise, the surface must be subdivided into elements over which the assumption of uniform intensity is valid. The reflected intensity  $I_{Rn}$  for each of  $n$  surfaces is

$$I_{Rn} = I_{Dn} \rho \quad (8)$$

where  $I_{Dn}$  is the direct intensity incident on surface  $n$  and  $\rho$  is the diffuse global spectral reflectivity in the UVGI range.

The view factor from a differential element to a rectangular surface, through the corner and located perpendicular to the surface, is (Modest 1993)

$$F_{d1-2} = \frac{1}{2\pi} \left[ \begin{aligned} &\frac{X}{\sqrt{1+X^2}} \text{ATAN} \left( \frac{Y}{\sqrt{1+X^2}} \right) \\ &+ \frac{Y}{\sqrt{1+Y^2}} \text{ATAN} \left( \frac{X}{\sqrt{1+Y^2}} \right) \end{aligned} \right] \quad (9)$$

where

$$X = \text{height}/x,$$

$$Y = \text{length}/x,$$

$$x = \text{distance to the corner, perpendicular to the surface.}$$

By dividing a large rectangle into four smaller rectangles, the intensity along any perpendicular line intersecting the large rectangle can be determined. For points that are beyond the edges of the rectangular surface, ghost rectangles representing the nonexistent areas must be included and their intensity contribution subtracted from the total. View factor algebra can be used when surfaces must be subdivided into numerous smaller elements to account for uneven intensity contours. The references may be consulted for more details on view factor algebra (Modest 1993; Howell 1982; Seigel and Howell 1981).

Equation 9 can be used to compute a three-dimensional matrix defining the intensity field due to the first reflections. This matrix can then be used to compute both the average and integrated dose as described later.

For a rectangular duct such as that shown in Figure 8, there will be four surfaces (top, bottom, left, and right) but the model can be generalized to any number of surfaces. For example, a round duct could be approximated by a polygon with a sufficiently large number of sides. The reflected intensity  $I_R$  seen by a microbe at any  $x$ ,  $y$ ,  $z$  point will be the algebraic sum of those from all surfaces:

$$I_R = \sum_{i=1}^n I_{Rn} F_{d1-2, n} \quad (10)$$

where  $F_{n,d1-2}$  = view factor to  $n$  facing walls (up to four).

No account has been taken in the above model of reflected radiation that is reabsorbed by the lamp itself, but this will generally be negligible provided the lamp occupies a small fraction of the total enclosure volume. The above procedure also assumes reflectivity is diffuse. More commonly, reflec-

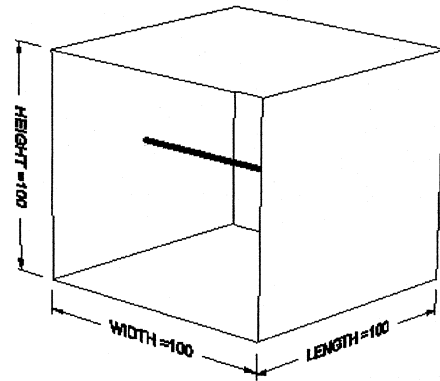


**Figure 8** Configuration of enclosure for the test case. All dimensions in cm. Lamp is 81.3 cm long and centered in duct. The four surfaces have 90% reflectivity and airflow is from left to right.

tive surfaces are specular, or mirrorlike. Analysis of specular reflections can be complex and, although some methods exist such as ray tracing techniques (Glassner 1989; Kowalski and Bahnfleth 2000), the assumption of diffuse surfaces will produce results that approach those of specular modeling provided lamps are spaced, not concentrated, and specular surfaces do not create focal points.

An alternative method for dealing with specular reflections, for a finite number of surfaces, is to apply Equation 4 for each specular reflection of the lamp. The lamp reflections must be reduced proportionally by the reflectivity of the surface. The inter-reflections can then be computed in a manner analogous to that described in the following section.

### The Inter-Reflected Intensity Field

When reflectivity is high (i.e., 75%-90% for aluminum paint) and the reflective surfaces enclose most of the chamber area, the subsequent reflections may contribute significantly to the total field. These reflections will bounce between the surfaces and are called inter-reflections. The intensity due to the inter-reflections achieves steady state literally at the speed of light, converging to a finite value that depends on geometry and reflectivity. The physical process of inter-reflections can be simulated by using a computer model and performing a sufficient number of iterations; usually only ten or less are sufficient.

Given that the surface intensities of the first reflections are known for all four surfaces from the preceding equations, each surface will then absorb some amount of energy from each of the other three surfaces. The amount of energy absorbed from the opposite (parallel) surface can be determined from Equation 9. For surfaces that are adjacent and perpendicular to each other, the following view factor can be used:

$$F_{d1-2} = \frac{1}{2\pi} \left[ \tan^{-1} \left( \frac{1}{Y} \right) - \frac{Y}{\sqrt{X^2 + Y^2}} \tan^{-1} \left( \frac{1}{\sqrt{X^2 + Y^2}} \right) \right] \quad (11)$$

The parameters in the above equation are defined as follows:

$$X = a/b$$

$$Y = c/b$$

where  $a$  = height,  $b$  = length, and  $c$  = perpendicular distance to surface.

Equations 9 and 11 can be used on each of the four surfaces in turn to determine the intensity received by each of the other three surfaces. The sum of the three contributions defines the incident energy on the surface. The amount actually reflected will be this total multiplied by the reflectivity, as in the first reflection case. The surface intensities computed represent the first inter-reflection.

To make accurate predictions with this method it is necessary to subdivide the surfaces into smaller elements and

compute the view factors and intensity contributions individually. This integrated sum will account for the variations in intensity across the surfaces.

The new surface intensities computed from the first inter-reflection can then be used to determine the next inter-reflection in an iterative fashion, simply by repeating this computational process. These computations should be performed for some ten or more reflections, at which point there will be little energy left to exchange. However, once the first two or three inter-reflections have been computed, the remaining inter-reflections can be computed by summing the resulting geometric series.

Consider the ideal case where the surface intensity from the first inter-reflection is uniform everywhere. The second inter-reflection intensity,  $I_{R2}$ , will be the product of the reflectivity, the total view factor, and the first inter-reflection surface intensity,  $I_{R1}$ , as follows:

$$I_{R2} = I_{R1} (\rho F_{tot}) \quad (12)$$

The third inter-reflection intensity,  $I_{R3}$ , will be the reflectivity times the view factor times the second inter-reflection as follows:

$$I_{R3} = I_{R2} (\rho F_{tot}) = I_{R1} (\rho F_{tot})^2 \quad (13)$$

Obviously, each subsequent inter-reflection will be the product of the reflectivity times the view factor, multiplied by the previous inter-reflection, in an infinite series. The total  $I_{Rtot}$  for all subsequent inter-reflections can be summed as

$$I_{Rtot} = I_{R1} (\rho F_{tot}) + I_{R1} (\rho F_{tot})^2 + I_{R1} (\rho F_{tot})^3 + \dots \quad (14)$$

This geometric series conveniently sums to

$$I_{Rtot} = I_{R1} \frac{\rho F_{tot}}{1 - \rho F_{tot}} \quad (15)$$

However, because the intensity field is not uniform for the first inter-reflection, Equation 15 cannot be used to compute the first or the second inter-reflection accurately. In fact, the first three inter-reflections need to be computed before Equation 15 can be applied, after which it will give the total reflected intensity from the fourth reflection onward.

The reason the geometric series approach works after three inter-reflections is because the effect of inter-reflection between surfaces is to average out the intensities and produce even intensity contours. In the example shown in Figure 9, the first two inter-reflections were used to compute the geometric series total for all the subsequent inter-reflections. The difference between these approaches was found to be only 0.05% after computing 30 inter-reflections between rectangular surfaces, each of which was subdivided into 10×20 elements.

A convenient way of computing the factor of reflectivity times the view factor in Equation 15 is to divide the third inter-reflection intensity by the second. This produces the following

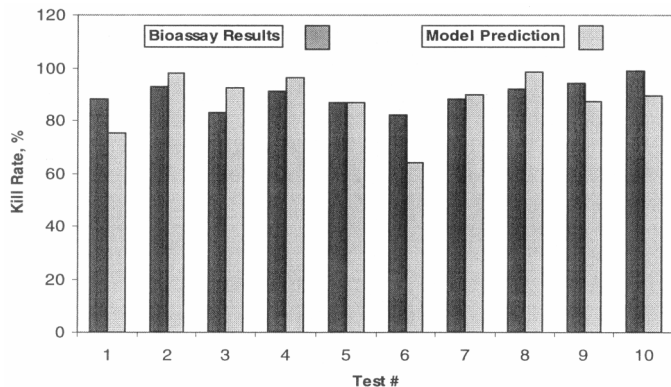


**Figure 9** Results of bioassays compared to predictions of model for kill rates with *Serratia marcescens* for various lamps and system configurations.

version of Equation 15 in which the total inter-reflection intensity is computed for reflections 3 through infinity:

$$\sum_{i=3}^{\infty} I_R = I_{R3} \frac{\frac{I_{R3}}{I_{R2}}}{1 - \frac{I_{R3}}{I_{R2}}} = \frac{(I_{R3})^2}{I_{R2} - I_{R3}} \quad (16)$$

The total for all inter-reflections then becomes

$$I_{R_{tot}} = I_{R1} + I_{R2} + I_{R3} + \frac{(I_{R3})^2}{I_{R2} - I_{R3}}. \quad (17)$$

The above methods can be used to compute the matrix of values defining the inter-reflection intensity field, which is then added (point-by-point) to the direct intensity field matrix and the first reflection intensity field matrix. Figure 10 shows the results of a detailed computation of the direct, reflected, and inter-reflections.

## VELOCITY PROFILES AND AIR MIXING

The duration of exposure and UVGI intensity determines the dose. Both depend on the velocity profile and amount of air mixing in the airstream. The velocity profile inside the duct or chamber depends on local conditions and may be impossible to define without CFD modeling. In any event, the design bulk velocity of a typical UVGI unit, approximately 2 m/s (400 fpm), ensures that sufficient mixing will occur and the effects of nonuniformity of the velocity profile will be moderated.

If the velocity profile is known, then it can be used to compute the integrated dose with the methods described herein. For all other applications, it is recommended that the velocity profile be assumed one-dimensional (i.e., constant and equal to the bulk velocity). If the engineer knows the velocity profile and it is nonuniform, then the lamps should probably be located in the highest velocity portion—this gives the lowest exposure time the highest intensity and vice-versa.

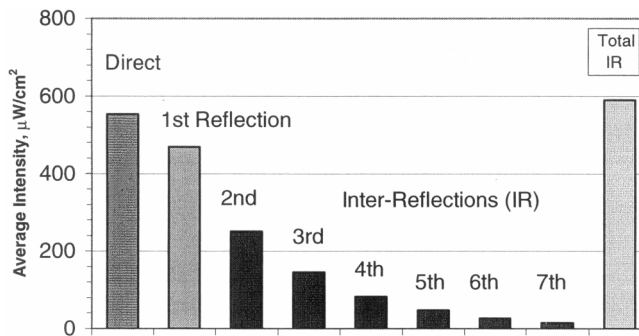


**Figure 10** Comparison of the direct and reflected average intensities predicted by the model for the test case. The total inter-reflections (Total IR) are computed from a geometric series.

Applications of these methods to upper air irradiation systems (First et al. 1999) are possible but for two confounding factors—unpredictable air movement and lamp fixtures with reflectors or baffles. The air movement in an occupied room would be difficult to predict even with CFD analysis, but some average degree of mixing could be assumed. The types of fixtures associated with upper air UVGI systems often include parabolic reflectors and baffles. Such complex geometries are difficult to analyze piecemeal with the methods presented here. A more feasible approach would be to use either empirical data or Monte Carlo methods (i.e., ray-tracing) as described earlier.

## LAMP PLACEMENT AND CONFIGURATION EFFICIENCY

Placement and selection of lamps can affect the overall disinfection rate for any given lamp power. If the intensity field is concentrated in one area, e.g., where several lamps are clustered, the intensity in that area may be much higher than is needed for disinfection—this represents an inefficiency.

On the other hand, if the intensity field is evenly distributed using numerous smaller lamps, then inefficiencies may be minimized. Another way to approximate this result is to use reflectors to redistribute the intensity field.

The general conclusion can be drawn that distributing the intensity field, through lamp location and reflective surfaces, will tend to increase the overall efficiency of the system, if it is not already as efficient as it can be. Theoretically, there must be some configuration of the lamps and the reflective enclosure that will provide a maximum efficiency of disinfection. At present, the only way to assess the efficiency of any system configuration is to use the methods presented to make comparisons and seek improvement. Ultimately, the system configuration will be determined by what combination is most cost-effective, and this will require comparisons of designs also.

## DISCUSSION

The modeling methodology described has been tested in two different laboratories in a series of bioassays sponsored by a leading manufacturer of UVGI systems. A proprietary software package that incorporates this methodology was used to predict disinfection rates for several duct configurations. Various lamp models, duct configurations, operating conditions, and test microbes were bioassayed with results mostly showing good agreement with model predictions. Many of the test results corroborated the model predictions within a few percent and average a conservative 90% or more.

Figure 10 shows the results for one set of tests performed on *Serratia marcescens* using a rectangular duct and various types and numbers of lamps or reflectivity. Airflows varied between tests. Although most results were within a few percent, occasional test results deviated significantly. The average error was 9% with a range of 0-19%.

The source of remaining error in the model may be due to relative humidity effects, shoulder effects, error in estimated rate constant, or other factors. No identifiable factors were found to have any relation to the residual errors. One factor not yet evaluated is shape of the microbe. Since most microbes are more spherical than planar, a view factor that addresses shape may offer some improvements to the model. View factors between arbitrarily oriented spheres and cylinders are not easily determined, even by numerical means, and this matter needs further study.

Some empirical evidence exists that spheres on the order of 1 cm absorb much more energy than a single planar photometer sensor for locations close to a source (Rahn et al. 1999). How much more a one-micron sphere might absorb in distances of a few centimeters from a source is an unresolved question at this time. Monte Carlo simulations of the spherical microbe problem have astronomical logistics and have not yet provided a solution.

Compounding the problem of spherical microbes is the fact that the rate constants are mostly based on plate culture tests. The true rate constant for an airborne microbe must be determined in air, but to do this requires precise knowledge of the intensity field. And so the model presented here may be useful for improving experimental determination of rate constants, which in turn may lead to an improved model.

## CONCLUSIONS

A methodology has been presented that predicts the performance of UVGI airstream disinfection systems. This method enables the design of more effective UVGI systems for any given application. Corroboration of the predictive capabilities of the model by laboratory tests has been promising, with most predictions falling within  $\pm 15\%$  of laboratory results. The ability to design systems effectively will contribute to lowered energy costs by avoiding the problems of over-design that are inherent in previous design methodologies.

Some areas remain that require further research in order to provide a complete understanding of UVGI system design

parameters and how they affect system efficiency. The effect of relative humidity on rate constants remains poorly understood. A model for specular reflectivity effects awaits development. Rate constants for microbial pathogens need reevaluation in airborne tests, and a more extensive database of rate constants is needed. Clearly there is a need for extensive new research in this area.

Finally, more experimental data on the shoulders and the second stage rate constants are needed, especially for the fungal and bacterial spores. Research in all these areas is ongoing but hardly adequate to meet the worldwide problem of airborne disease today. The authors hope the pace of such research will gain momentum and elevate UVGI system design from an art to an exact science.

## ACKNOWLEDGMENTS

This research was supported by a private grant from Ultraviolet Devices, Inc. (UVDI) of Valencia, California. We also thank UVDI for their kind permission to use their proprietary software and for providing photosensor data, the results of laboratory bioassays, and the rate constant data for *Serratia marcescens*. Thanks also to Mark Hernandez of the University of Colorado for helpful input and to Richard Mistrick of Penn State for originally suggesting the view factor model.

## REFERENCES

- ASHRAE. 1991. *1991 ASHRAE Handbook—HVAC Applications*. Atlanta: American Society of Heating, Refrigerating and Air-Conditioning Engineers, Inc.
- Asthana, A., and R.W. Tuveson. 1992. Effects of UV and phototoxins on selected fungal pathogens of citrus. *Int. J. Plant Sci.* 153 (3): 442-452.
- AWWA. 1971. *Water quality and treatment*. American Water Works Association, editor. New York: McGraw-Hill.
- Cerf, O. 1977. A review: Tailing of survival curves of bacterial spores. *J. Appl. Bact.* 42: 1-19.
- Collins, F.M. 1971. Relative susceptibility of acid-fast and non-acid fast bacteria to ultraviolet light. *Appl. Microbiol.* 21: 411-413.
- Davidovich, I.A., and G.P. Kishchenko. 1991. The shape of the survival curves in the inactivation of viruses. *Mol. Gen., Microb. & Virol.* 6: 13-16.
- First, M.W., E.A. Nardell, W. Chaisson, and R. Riley. 1999. Guidelines for the application of upper-room ultraviolet germicidal irradiation for preventing transmission of airborne contagion. *ASHRAE Journal* 105.
- Gates, F.L. 1929. A study of the bactericidal action of ultraviolet light. *J. Gen. Physiol.* 13: 231-260.
- Glassner, A.S., ed. 1989. *An introduction to ray tracing*. London: Academic Press.
- Hollaender, A. 1943. Effect of long ultraviolet and short visible radiation (3500 to 4900) on *Escherichia coli*. *J. Bact.* 46: 531-541.

- Howell, J.R. 1982. *A catalog of radiation view factors*. New York: McGraw-Hill.
- IES. 1981. *Lighting handbook reference volume*. Illumination Engineering Society.
- Jensen, M.M. 1964. Inactivation of airborne viruses by ultraviolet irradiation. *Applied Microbiology* 12 (5): 418-420.
- Koch, A.L. 1995. *Bacterial growth and form*. New York: Chapman & Hall.
- Kowalski, W.J., and W.P. Bahnfleth. 2000. UVGI design basics for air and surface disinfection. *HPAC* 72 (1).
- Lidwell, O.M., and E.J. Lowbury. 1950. The survival of bacteria in dust. *Annual Review of Microbiology* 14: 38-43.
- Luciano, J.R. 1977. *Air contamination control in hospitals*. New York: Plenum Press.
- Luckiesh, M. 1946. *Applications of germicidal, erythematous and infrared energy*. New York: D. Van Nostrand Co.
- Luckiesh, M., and L.L. Holladay. 1942. Designing installations of germicidal lamps for occupied rooms. *General Electric Review* 45 (6): 343-349.
- Modest, M.F. 1993. *Radiative heat transfer*. New York: McGraw-Hill.
- Philips. 1985. *Germicidal lamps and applications*. Philips Lighting Division.
- Qualls, R.G. and J.D. Johnson. 1983. Bioassay and dose measurement in UV disinfection. *Appl. Microb.* 45 (3): 872-877.
- Qualls, R.G. and J.D. Johnson. 1985. Modeling and efficiency of ultraviolet disinfection systems. *Water Res.* 19 (8): 1039-1046.
- Rahn, R.O., X. Peng, and S.L. Miller. 1999. Dosimetry of room-air germicidal (254 nm) radiation using spherical actinometry. 70 (3): 314-318.
- Rentschler, H.C, and R. Nagy. 1940. Advantages of bactericidal ultraviolet radiation in air conditioning systems. *HPAC* 12: 127-130.
- Riley, R.L., and J.E. Kaufman. 1972. Effect of relative humidity on the inactivation of airborne *Serratia marcescens* by ultraviolet radiation. *Applied Microbiology* 23 (6): 1113-1120.
- Riley, R.L., and F. O'Grady. 1961. *Airborne infection*. New York: The Macmillan Company.
- Riley, R.L, and E.A. Nardell. 1989. Clearing the air: The theory and application of ultraviolet disinfection. *Am. Rev. Resp. Dis.* 139: 1286-1294.
- Severin, B.F., M.T. Suidan, and R.S. Englebrecht. 1983. Kinetic modeling of U.V. disinfection of water. *Water Res.* 17 (11): 1669-1678.
- Siegel, R., and J.R. Howell. 1981. *Thermal radiation heat transfer*. New York: Hemisphere.
- Sharp, G. 1939. The lethal action of short ultraviolet rays on several common pathogenic bacteria. *J. Bact.* 37: 447-459.
- Sharp, G. 1940. The effects of ultraviolet light on bacteria suspended in air. *J. Bact.* 38:535-547.
- Whiting, R.C. 1991. Predictive modeling. In: Doyle, M.P., ed., *Food microbiology*, pp. 728-739. Washington: ASM Press.